Modulation instability in noninstantaneous Kerr media with walk-off and cross-phase modulation for mixed group-velocity-dispersion regimes

Askery Canabarro,[1,2,*] B. Santos,[3] B. de Lima Bernardo,[4] André L. Moura,[1,5] W. C. Soares,[1] E. de Lima,[1] Iram Gléria,[6] and M. L. Lyra[6]

[1]*Grupo de Física da Matéria Condensada, Núcleo de Ciências Exatas, Campus Arapiraca, Universidade Federal de Alagoas, 57309-005 Arapiraca-AL, Brazil*

[2]*Center for Polymer Studies and Department of Physics, Boston University, 590 Commonwealth Avenue, Boston, Massachusetts 02215, USA*

[3]*Observatório Nacional, 20921-400 Rio de Janeiro–RJ, Brazil*

[4]*Department of Physics, Harvard University, Cambridge, Massachusetts 02138, USA*

[5]*Departamento de Física, Universidade Federal de Pernambuco, 50670-901 Recife, PE, Brazil*

[6]*Instituto de Física, Universidade Federal de Alagoas, 57072-970 Maceió-AL, Brazil*

(Received 21 October 2015; published 23 February 2016)

Taking into account relaxing Kerr nonlinearity and walk-off effects, the conditions and gain spectra of cross-phase modulation-induced modulational instability (XPM-MI) of two incoherently copropagating optical waves of different frequencies and same polarization are investigated. We devote particular attention to the mixed case in which one pulse propagates under the normal group-velocity dispersion (GVD) regime, while the second one is under an anomalous GVD regime. We unveil that in the limit of an instantaneuous nonlinear response, the typical frequency with maximum gain converges to a finite value in the mixed GDV regime, while it continuously grows with the group-velocity mismatch in the normal GVD regime. As a result, the maximum gain typically decreases with the group-velocity mismatch in the mixed regime, contrasting with the opposite trend in the normal GVD regime. Further, we show that besides the mode having maximum gain at a frequency decaying with $1/\tau^{1/3}$ in the slow response limit, there is a second mode having maximum gain with a distinct scaling behavior $\Omega_{\max} \propto 1/\tau$ in the absence of group-velocity mismatch. The associated maximum gains scale, respectively, as $1/\tau^{2/3}$ and $1/\tau$, thus signaling the corresponding quadratic and linear dispersion relation of these modes in the low-frequency limit. A detailed analysis of the influence of the nonlinear response time and group-velocity dispersion on the MI gain spectrum is also provided.

DOI: 10.1103/PhysRevA.93.023834

I. INTRODUCTION

The optical nonlinear properties of amorphous materials have been extensively studied due to their vast potential in practical applications along with a great deal of interesting fundamental features. One of their most representative members is the silica. However, there is a consensus that silica fibers do not present any even-order nonlinearity, although the induction of stable second-order nonlinearity in silicate glasses has been demonstrated [1,2]. Therefore, in general, the lowest nonlinear susceptibility present is the third-order one, and practically all nonlinear effects observed in fibers used in telecommunication systems are related to the $\chi^{(3)}$ tensor. The copropagation of two intense optical beams in such media may lead to many fascinating effects such as modulational instability (MI), stimulated Raman scattering (SRS), stimulated Brillouin scattering, four-wave mixing, and many others.

Under appropriate conditions, a great variety of nonlinear dispersive systems exhibit modulation instability, which corresponds to the exponential growth of weak perturbations, breaking a continuous-wave (cw) or quasi-cw wave in a train of solitonlike pulses [3–6]. In the temporal domain, MI materializes itself as a result of the interplay between nonlinearity and group-velocity dispersion (GVD): anomalous group-velocity dispersion for self-phase modulation and both anomalous and normal group-velocity dispersion for cross-phase modulation (XPM). This instability occurs in diverse physical fields and may correspond to the fundamental physical mechanism igniting unique processes such as spin waves in magnetic films, solitons, and rogue waves [7–17]. Furthermore, among the vast technological applications of MI we can cite the measurement of optical fiber parameters [18], the creation of all-optical switches [19], the construction of fiber lasers [20,21], and the control of nonlinearity-managed optical media [22].

From a theoretical perspective, the description of the evolution of copropagating pulses is made by using extensions of the nonlinear Schrödinger equation (NLSE), whose analytical results provide the dispersion relation, the unstable conditions, as well as the gain spectra. This class of models for the copropagation of pulses has been the theoretical background of several experimental studies [23–25]. In recent years, a large variety of physical properties was incorporated in the model such as higher-order dispersion [26–28]; multiple optical beams [29]; cubic, quadratic, and quintic nonlinearities; negative index material [30–35]; saturable nonlinearity [35–38]; and noninstantaneous nonlinear response [25,38–47]. Due to the inadequacy of the conventional instantaneous Kerr nonlinearity for ultrashort pulses and highly dispersive media, the delayed nonlinear response must be considered. This

*Corresponding author: askery.canabarro@arapiraca.ufal.br

delayed nonlinear response can be incorporated by including additional terms corresponding to the Taylor expansion of the delayed envelope amplitude in the NLSE, which is a good approximation only for the low-frequency regime, not being valid for high frequencies. Therefore, models incorporating a Debye relaxation of the nonlinear response are considered to be more reliable regardless of the frequency regime [38–47].

Recently, a method to obtain slow light from noninstantaneous MI has been theoretically proposed [48]. There, a straight incident light beam is used as the pump wave, whereas a much less intense oblique incident one is the plane signal wave to be modulated. It is also demonstrated that the group velocity is tunable in such a system. From the practical point of view, with the improvements in the fabrication of highly noninstantaneous Kerr media [49], the conventional Kerr response must be replaced, demanding a better understanding of the problem. It is also important to mention the fundamental role played by XPM between signal and probe beams as a tool for realizing quantum nondemolition measurements [50–52], which, in turn, have opened the way for future applications in photonic quantum communication systems and quantum information processing [53,54].

Notwithstanding the myriad of previous works devoted to investigate distinct aspects of nonlinear pulse propagation, one still lacks a full understanding of the main basic physical processes for the case of noninstantaneous responding media. Here, we include both the XPM and delayed nonlinear response contributions to extensions of the nonlinear Schrödinger equation in order to study the MI of incoherently coupled copropagating beams in optical fibers with noninstantaneous Kerr response. The combined effects of relaxing nonlinearity, group-velocity mismatch (GVM), and XPM has been previously addressed in Ref. [40] for the particular case of both pulses experiencing normal GVD. However, as emphasized in Ref. [25], a complete characterization of the modulational instability process requires the investigation of the anomalous dispersion regime on which quite new physical aspects can emerge.

In this paper, by considering the importance of XPM and walk-off effects in the MI dynamics [55–61], we investigate the interplay between the XPM and walk-off effect in the MI spectrum in the system of relaxing nonlinear response for the case in which one of the beams experiences the normal GVD regime and the other beam is propagating in the anomalous GVD regime. This situation is particularly important, for example, in the realization of a nondemolition measurement of a signaling pulse whose frequency is considerably different from that of the probe, inasmuch as both pulses propagate through the nonlinear medium under distinct GVD regimes. Specifically, the main characteristic of the MI gain spectrum will be analyzed as a function of the characteristic response time and GVM.

II. THEORETICAL MODEL AND LINEAR STABILITY ANALYSIS

We consider the case in which two optical pulses of different frequencies and identical polarizations are incident on a single-mode optical fiber with Kerr nonlinearity, which is described by the following set of coupled nonlinear Schrödinger equations (CNLSEs) [3,37,55–57,62]:

$$\begin{aligned} i\left(\frac{\partial E_1}{\partial z}+\frac{\delta}{2}\frac{\partial E_1}{\partial t}\right) &= \frac{\beta_1}{2}\frac{\partial^2 E_1}{\partial t^2}-\gamma_1(|E_1|^2+2|E_2|^2)E_1, \\ i\left(\frac{\partial E_2}{\partial z}-\frac{\delta}{2}\frac{\partial E_2}{\partial t}\right) &= \frac{\beta_2}{2}\frac{\partial^2 E_2}{\partial t^2}-\gamma_2(|E_2|^2+2|E_1|^2)E_2, \end{aligned} \tag{1}$$

where $E_i = E_i(t,z)$ represents the electric field envelope of the ith wave propagating along the z axis with a group velocity v_{gi} $(i = 1,2)$. We are assuming a retarded time reference frame $t = T - z/\bar{v}_g$ moving with the average group velocity $1/\bar{v}_g = (1/v_{g1} + 1/v_{g2})/2$. β_i is the GVD coefficient, and γ_j is the Kerr parameter of the fiber experienced by this particular beam. The GVM is represented by δ, where $\delta = | v_{g1}^{-1} - v_{g2}^{-1} |$. The factor 2 before the XPM terms accounts for the assumption that the two beams have the same polarization.

The above relations describe the propagation of pulses strictly in the instantaneous nonlinear response. Roughly speaking, for the case of ultrashort pulse propagation, besides the instantaneous response due to electronic contribution, the slow response of thermal origin or reorientational nonlinearity, whose time scale may vary from picoseconds to nanoseconds, must be considered. The origin of such delayed effects is in general assumed to be due to the vibrational Raman effect. In describing such effects, we adopt a simple relaxational model known as the Debye relaxational model, whose applicability is known to be valid independent of the frequency regime. The relaxation coefficient in this model represents the finite response time inherent of the nonlinear material.

For the usual Kerr response, the medium exhibits an instantaneous response which is given by

$$P \propto |E|^2 E, \tag{2}$$

with P being the nonlinear polarization. Nevertheless, in the Debye relaxation model, the medium has a finite response time τ. This feature is effectively taken into account by writing $P \propto \chi(E,t)E$, where the rate at which χ varies on time is given by

$$\frac{\partial \chi}{\partial t} = -\frac{1}{\tau}\chi + \frac{1}{\tau}|E|^2, \tag{3}$$

which describes the exponential relaxation of the nonlinear contribution to its stationary solution. Thus, a time-dependent nonlinear response can be incorporated in the system of CNLSEs, which in turn are expressed as [38–47]

$$\begin{aligned} i\left(\frac{\partial E_1}{\partial z}+\frac{\delta}{2}\frac{\partial E_1}{\partial t}\right) &= \frac{\beta_1}{2}\frac{\partial^2 E_1}{\partial t^2}-\gamma_1 N_1 E_1, \\ i\left(\frac{\partial E_2}{\partial z}-\frac{\delta}{2}\frac{\partial E_2}{\partial t}\right) &= \frac{\beta_2}{2}\frac{\partial^2 E_2}{\partial t^2}-\gamma_2 N_2 E_2, \\ \frac{\partial N_1}{\partial t} &= \frac{1}{\tau}(-N_1+|E_1|^2+2|E_2|^2), \\ \frac{\partial N_2}{\partial t} &= \frac{1}{\tau}(-N_2+2|E_1|^2+|E_2|^2), \end{aligned} \tag{4}$$

with $N = N(z,t)$ describing the nonlinear index of the medium. The parameter τ corresponds to the finite response time. Therefore, it was shown that it reaches the usual Kerr response in the limit when $\tau \to 0$. This is also valid when the slowly varying envelope approximation does not hold [47].

Then, it will be shown that the regimes of slow and fast response times (large and small values of τ, respectively) lead to distinct outcomes.

The steady state can be easily found as the time-independent solution of Eq. (4) which is given by $E_1 = E_1^0 e^{[i\gamma_1(|E_1^0|^2+2|E_2^0|^2)z]}$, $E_2 = E_2^0 e^{[i\gamma_2(2|E_1^0|^2+|E_2^0|^2)z]}$, $N_1 = |E_1^0|^2 + 2|E_2^0|^2$, and $N_2 = 2|E_1^0|^2 + |E_2^0|^2$. Hereafter, E_1^0 and E_2^0 will be considered as real stationary field amplitudes for simplicity. In order to investigate the effect of the small harmonic perturbations against the steady-state solution of the above dynamical equations, we make use of a linear stability analysis. We assume that

$$\begin{aligned} E_1 &= \left[E_1^0 + e_1(z,t)\right]e^{[i\gamma_1(|E_1^0|^2+2|E_2^0|^2)z]}, \\ E_2 &= \left[E_2^0 + e_2(z,t)\right]e^{[i\gamma_2(2|E_1^0|^2+|E_2^0|^2)z]}, \\ N_1 &= n_1(z,t) + \left|E_1^0\right|^2 + 2\left|E_2^0\right|^2, \\ N_2 &= n_2(z,t) + 2\left|E_1^0\right|^2 + \left|E_2^0\right|^2, \end{aligned} \tag{5}$$

with $e_j(z,t)$ as a weak perturbation which satisfies $|e_j(z,t)|^2 \ll |E_j^0|^2$, and $n_j(z,t)$ as a small perturbation to the stationary nonlinearity. Also, by substituting Eqs. (5) in (4), we can derive the linearized equations satisfying the perturbations $e_j(z,t)$ and $n_j(z,t)$, which yields

$$\begin{aligned} i\frac{\partial e_1}{\partial z} + \frac{i}{v_{g1}}\frac{\partial e_1}{\partial t} &= \frac{1}{2}\beta_1\frac{\partial^2 e_1}{\partial t^2} - \gamma_1 n_1 E_1^0, \\ i\frac{\partial e_2}{\partial z} + \frac{i}{v_{g2}}\frac{\partial e_2}{\partial t} &= \frac{1}{2}\beta_2\frac{\partial^2 e_2}{\partial t^2} - \gamma_2 n_2 E_2^0, \\ \frac{\partial n_1}{\partial t} &= \frac{1}{\tau}\left[-n_1 + E_1^0(e_1+e_1^*) + 2E_2^0(e_2+e_2^*)\right], \\ \frac{\partial n_2}{\partial t} &= \frac{1}{\tau}\left[-n_2 + 2E_1^0(e_1+e_1^*) + E_2^0(e_2+e_2^*)\right]. \end{aligned} \tag{6}$$

The solution for this system of coupled complex linear equations can be simply achieved after performing proper mathematical transforms (Fourier transform in time with components having a real modulation frequency Ω and Laplace transform in space with components having a complex wave number k). Thus, expressing the decomposition of the perturbations as

$$\begin{aligned} e_j(z,t) &= \frac{1}{\sqrt{2\pi}}\int e^{-ikz}e^{i\Omega t}\widehat{e}_j(\Omega,k)dk\,d\Omega, \\ n_j(z,t) &= \frac{1}{\sqrt{2\pi}}\int e^{-ikz}e^{i\Omega t}\widehat{n}_j(\Omega,k)dk\,d\Omega, \end{aligned} \tag{7}$$

simple relations for the components can be obtained. In what follows, we examine the extent to which the effects of XPM and noninstantaneous response interfere in this specific case that modulations with equal wave vectors are associated to each beam. In Ref. [58] a method is demonstrated to extend the present case to the general one. After eliminating $\widehat{n}_j(\Omega,k)$, the amplitude of the harmonic components of the perturbation fields can be found to be coupled as follows:

$$\begin{aligned} &\left(k - \frac{\Omega}{v_{g1}} + \beta_1\frac{\Omega^2}{2}\right)\widehat{e}_1(\Omega,k) + \frac{\gamma_1 E_1^0}{(i\Omega\tau+1)}\{E_1^0[\widehat{e}_1(\Omega,k) \\ &\quad + \widehat{e}_1^*(-\Omega,-k)] - 2E_2^0[\widehat{e}_2(\Omega,k) + \widehat{e}_2^*(-\Omega,-k)]\} = 0, \\ &\left(k - \frac{\Omega}{v_{g2}} + \beta_2\frac{\Omega^2}{2}\right)\widehat{e}_2(\Omega,k) + \frac{\gamma_2 E_2^0}{(i\Omega\tau+1)}\left\{2E_1^0[\widehat{e}_1(\Omega,k)\right. \\ &\quad \left. + \widehat{e}_1^*(-\Omega,-k)] - E_2^0[\widehat{e}_2(\Omega,k) + \widehat{e}_2^*(-\Omega,-k)]\right\} = 0. \end{aligned} \tag{8}$$

In a similar fashion, the conjugate of Eq. (8) provides the counterpart equations for the complex conjugate of these perturbation fields. After some calculations, it can be seen that the system of four homogeneous equations for e_1, e_1^*, e_2, and e_2^*, given by Eqs. (8) and the corresponding complex conjugates, presents a nontrivial solution only when the dispersion relation is satisfied by the parameters k and Ω, which is given by

$$\left[\left(k - \frac{\Omega}{v_{g1}}\right)^2 - f_1\right]\left[\left(k - \frac{\Omega}{v_{g2}}\right)^2 - f_2\right] = C_{\mathrm{XPM}}, \tag{9}$$

where

$$f_j = \frac{\beta_j\Omega^2}{2}\left(\frac{\beta_j\Omega^2}{2} + \frac{2\gamma_j\left|E_j^0\right|^2}{1+i\Omega\tau}\right). \tag{10}$$

The coupling parameter C_{XPM} is given by

$$C_{\mathrm{XPM}} = \frac{4\gamma_1\gamma_2\beta_1\beta_2\left|E_1^0\right|^2\left|E_2^0\right|^2\Omega^4}{(1+i\Omega\tau)^2}. \tag{11}$$

The above dispersion relation [Eqs. (9)–(11)] determines the stability of the steady-state solution against harmonic perturbations. These become exponentially unstable whenever the wave number k exhibits an imaginary term, with the modulational instability gain being defined as $g(\Omega = 2\,\mathrm{Im}k$. Different MI gain spectra correspond to distinct solutions of this equation and one can examine qualitatively and quantitatively the main role played by the nonlinear response time.

For the case of instantaneous nonlinear response ($\tau = 0$), one can note that the dispersion relation is a fourth-order polynomial in k with real coefficients leading to four solutions. Two of the solutions are always real and thus completely irrelevant to MI investigations, and the other two can be a complex conjugate pair, thereby being responsible for the MI dynamics and thus providing the emergence of, in general, only one unstable gain sideband, as extensively seen in many previous works [3,37,40,55–57,62].

On the other hand, by adding a response time in the nonlinear response ($\tau \neq 0$), it is evident from the dispersion relation that the terms f_i [Eq. (10)] and C_{XPM} [Eq. (11)] become complex numbers, thus producing an imaginary part to the wave number k and expanding the frequency range of unstable harmonic perturbations [38–44]. In fact, for any finite value τ, Eqs. (9)–(11) account for a fourth-order polynomial equation with complex coefficients. Since the complex roots do not necessarily appear in conjugate pairs, this leads to the possibility of up to four unstable modes for a given frequency Ω [40]. More detailed discussions are presented in Secs. III B and III C.

Thus, the incorporation of delay in the XPM leads to two unstable modes in contrast to a single unstable mode in the case of an instantaneously responding medium. The interplay of XPM, walk-off effect, and delayed nonlinear response in the coupled system can be analyzed by numerically solving the dispersion relation equation to obtain the gain spectrum. Therefore, we organized our analysis in three parts: (a) study of the effect of walk-off on the XPM-MI spectrum, (b) analysis of the impact of a finite relaxation time on the MI dynamics, and (c) investigation of the of interplay of both of these effects. Furthermore, in order to give a complete picture of the role of walk-off and delayed nonlinear response in the XPM-induced MI dynamics, we consider the case in which one of the beams propagates in normal GVD regime and the other beam runs under the anomalous GVD regime.

In the following results, we use the dispersion parameters as $\beta_1 = -\beta_2$, with $\beta_1 = \pm 0.06\ \mathrm{ps^2\,m^{-1}}$ and the nonlinear parameters $\gamma_1 = \gamma_2 = 0.015\ \mathrm{W^{-1}\,m^{-1}}$. The input optical powers are set as $P_1 = 100$ W and $P_2 = \epsilon P_1$, where $\epsilon = 1$, except as otherwise stated. Moreover, $\nu_1 = 1$ m/ps, the group-velocity mismatch varies in the range $\delta = 0$–$10\ \mathrm{ps\,m^{-1}}$, and the delay parameters range in the interval $\tau = 0$–10 ps.

III. RESULTS AND DISCUSSIONS

In this work we intend to provide a detailed analysis of the interplay between walk-off and noninstantaneous Kerr response for the case in which one of the beams is experiencing normal GVD and the other beam undergoes anomalous GVD ($\beta_1\beta_2 < 0$). For the sake of clarity, the particularities of each physical effect are discussed separately in the following subsections.

A. Walk-off effect on XPM

To illustrate the role of the walk-off effect in the XPM-MI, let us consider the case of instantaneous nonlinear response ($\tau = 0$). Here, we investigate the walk-off effect in the case in which one of the beams experiences normal GVD and the other beam anomalous GVD ($\beta_1\beta_2 < 0$).

In the absence of GVM ($\delta = 0$), the MI spectrum extends over all frequencies. This feature would imply in the generation of an infinitely wide sideband which is not observed in practical situations. However, for any non-null value of δ the MI instability band acquires a finite range. As δ is further increased, the MI band is shifted toward lower frequencies and its range is reduced, narrowing the band. Moreover, the maximum value of the gain decreases, reaching a saturation as a function of δ, as is evident from Fig. 1 (top). As it will be better analyzed ahead, for $\delta < \delta_c \approx 0.4\ \mathrm{ps\,m^{-1}}$ two maxima can be seen. We have plotted a qualitative study of this behavior in Fig. 1 (bottom), where the two bands can be seen for every chosen value of the GVM: one with large values of the maximum gain occurring in high frequencies and the other taking place for lower frequencies with smaller corresponding peaks. Note that both the peaks and their corresponding frequencies are reduced with increasing δ.

The qualitative picture of the role of GVM on MI plotted in Fig. 1 can be better analyzed by exploring the dependence of the local gain maxima on the GVM. Figure 2 depicts the

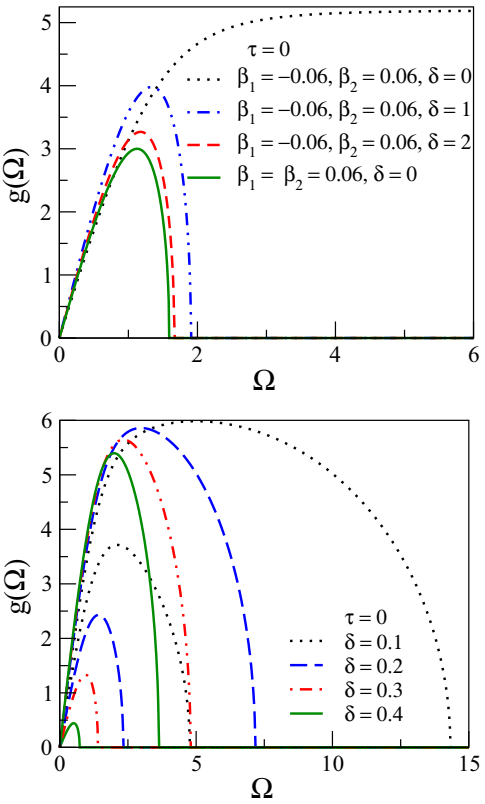

FIG. 1. MI gain spectra g ($\mathrm{m^{-1}}$) as a function of the frequency Ω (THz) with the effect of GVM for different values of δ ($\mathrm{ps\,m^{-1}}$) for instantaneous nonlinear response ($\tau = 0$ ps). Top: $\beta_1 = \beta_2 = 0.06\ \mathrm{ps^2\,m^{-1}}$ (solid line) and $\beta_1 = -0.06\ \mathrm{ps^2\,m^{-1}}$, $\beta_2 = 0.06\ \mathrm{ps^2\,m^{-1}}$ otherwise. Bottom: $\beta_1 = -0.06\ \mathrm{ps^2\,m^{-1}}$ and $\beta_2 = 0.06\ \mathrm{ps^2\,m^{-1}}$.

local maximum gain and the corresponding frequency in each instability band for all possible combinations of GVD regimes of the propagating pulses for the case of instantaneous Kerr response ($\tau = 0$).

When both beams experience the normal GVD regime ($\beta_1 = \beta_2 = 0.06\ \mathrm{ps^2\,m^{-1}}$), just one MI band is present and its peak increases with GVM [40,55–57], saturating after some value of δ, as it can be inferred from Fig. 2 (pluses, top). Withal, the situation is somewhat different for the case of mixed GVD regimes. Here, for small values of δ ($\delta < \delta_c \approx 0.4\ \mathrm{ps\,m^{-1}}$), two peaks are present and their values, $g_{\max}$, decrease monotonically, apart from the very small values of δ and the greatest peak. Notice that the values for smaller peaks decrease almost linearly with δ for the two-band condition ($\delta < \delta_c$). Furthermore, for larger values of δ we can see just one peak which also reaches a plateau with increasing values of δ [compare pluses and circles in Fig. 2 (top)]. This scenario is well distinct from the case of both pulses experiencing the normal GVD regime [40,55–57].

The frequency at which the gain in the instantaneous ($\tau = 0$) band is maximum does increase linearly with GVM [see pluses in Fig. 2 (bottom)] when both pulses experience normal GVD regime, as pointed out in Refs. [40,55–57]. On the other hand, for the case of mixed GVD regimes ($\beta_1\beta_2 < 0$) there are two spectral MI bands, as already mentioned before, whose

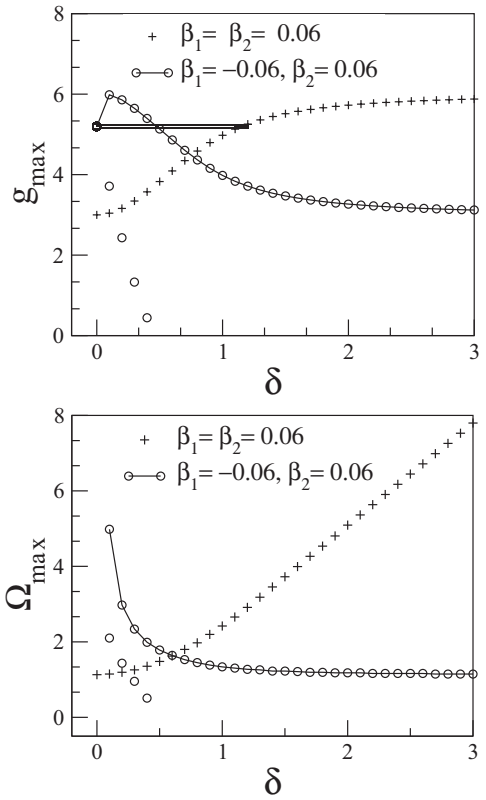

FIG. 2. Local maximum gain $g_{\max}$ (m^{-1}) and its corresponding frequency $\Omega_{\max}$ (THz) for each instability branch as a function of the GVM δ (ps m^{-1}) and conventional Kerr response $\tau = 0$ ps for the case of both beams in the normal GVD regime (pluses) and mixed GVD regime (circles). The other parameters are the same as those used in the previous figure.

peaks rapidly decay with δ. The corresponding frequencies at which those maxima occur are also different from each other, as can be deduced from Fig. 2 (bottom). However, if $\delta > 0.4$ ps m^{-1}, just one MI band occurs and its frequency is practically independent of the GVM parameter. It is worth mentioning that this delimiting value for the GVM (δ_c) depends on all parameters used and it was not further investigated in this work.

B. Relaxing nonlinearity effect on XPM

In this subsection, we turn our attention to the specific role played by the delayed nonlinear response in XPM-MI. Thus, we restrict our analysis to the case of null group-velocity mismatch ($\delta = 0$).

In the seminal works of Agrawal for the XPM coupling of pulses in the normal GVD regime [55–57] just one instability band was present once the dispersion relation accounted for a second degree polynomial equation with real coefficients. As addressed before, the addition of a response time in the nonlinear response ($\tau \neq 0$) turns the dispersion relation terms f_i and C_{XPM} of Eq. (9) into complex numbers. In addition, for $\delta = 0$ and $|\beta_1| = |\beta_2|$ (as used for the elaboration of Fig. 3), Eq. (9) can be reduced to a second-order polynomial equation. Observe that for $\tau \neq 0$ two spectral bands are present. This new band appears only due to the noninstantaneous nonlinear

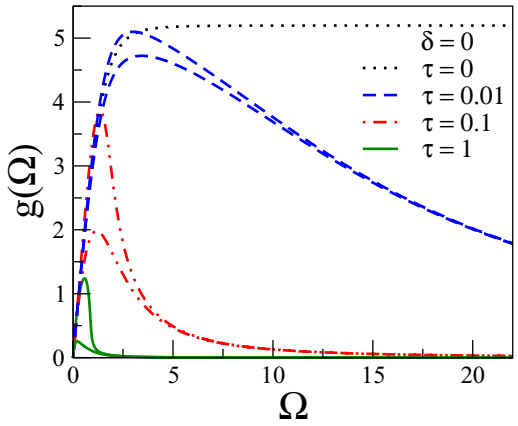

FIG. 3. MI gain spectra g (m^{-1}) as a function of the frequency Ω (THz) for several values of the nonlinear delay parameter τ (ps) when $\delta = 0$ ps m^{-1}. The other parameters are the same as those used in previous figures.

response. Therefore, the delay in the nonlinear response is responsible for the appearance of Raman bands besides the conventional one.

In Fig. 3 it is possible to qualitatively understand the main role played by the delayed nonlinear response. The noninstantaneous parameter not only induce a new instability band, but also reduces their peaks in comparison to the instantaneous band and moves their corresponding frequencies to lower values, a behavior similar to what is observed when one is dealing with saturable response [35–38]. We can also notice that the situation is distinct for small and large values of τ, corresponding to fast and slow delayed nonlinear responses, respectively.

A detailed analysis of the relation of the peaks of the gain and their corresponding frequencies with the noninstantaneous response is shown in Fig. 4, where the local maxima of $g(\Omega)$ and their corresponding frequencies are plotted for each instability branch as a function of the response time τ and null GVM ($\delta = 0$). In the regime of fast nonlinear responses (small τ), the two peaks show practically the same value and they are roughly independent of $\tau < \tau_c' \approx 0.01$ [see the region for $\tau < \tau_c'$ in Fig. 4 (top)]. For large values of τ the situation is different: the peaks decay as $1/\tau$ for one band and as $1/\tau^{2/3}$ for the other. The frequency at which the gain in the instantaneous band is maximum decays monotonically with τ [see Fig. 4 (bottom)]. Again we can clearly see two well distinct regimes for fast and slow nonlinear response. In the region of fast response, the two frequencies are almost indistinguishable decaying as $1/\tau^{1/3}$. However, for $\tau > \tau_c''$ (slightly larger than the previous one), the frequencies become distinguishable: one frequency still decaying as $1/\tau^{1/3}$, and the other one in the other band decaying faster as $1/\tau$. These asymptotic behaviors can be understood by analyzing the dispersion relation [Eqs. (9)–(11)]. One of the asymptotic solutions having maximum gain is such that the two terms within the brackets in Eq. (10) are of the same magnitude. This implies that $\Omega_{\max}^2 \propto 1/\Omega_{\max}\tau$ or, equivalently, $\Omega_{\max} \propto 1/\tau^{1/3}$. This solution has a quadratic dispersion relation thus leading to $g_{\max} \propto \Omega_{\max}^2 \propto 1/\tau^{2/3}$. On the other hand, the second

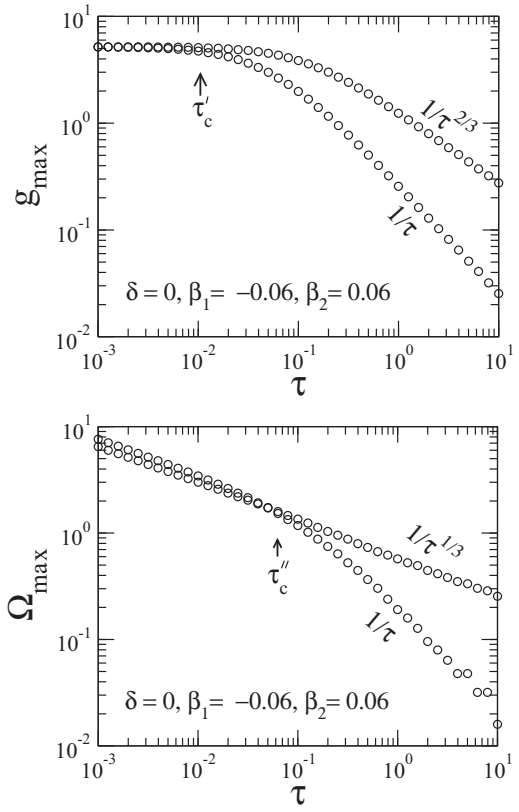

FIG. 4. Local maximum gain g_{max} (m^{-1}) and its corresponding frequency Ω_{max} (THz) for each instability branch as a function of the response time τ (ps) and null GVM ($\delta = 0\,ps\,m^{-1}$) for the case of mixed GVD regimes (circles). The other parameters are the same as those used in previous figures. τ_c' and τ_c'' stand for the crossover response times in the maximum gain and frequency, respectively.

maximum gain is related to a solution with $\Omega_{max}\tau$ remaining constant as τ increases and has a linear dispersion. As a result, $g_{max} \propto \Omega_{max} \propto 1/\tau$, as illustrated in Fig. 4.

C. Interplay between walk-off and noninstantaneous Kerr effects

Taking into account the results of the previous section, we organized our analysis of the joint effects of both noninstantaneous Kerr response $\tau \neq 0$ and group-velocity mismatch $\delta \neq 0$. From the mathematical point of view, the dispersion relation is again a fourth-order polynomial equation with complex coefficients, opening the possibility of up to four modes with distinct gain spectra. In Fig. 5 we provide an overview of this interplay. Notice that for $\tau = 0.1$ and $\tau = 0.01$ one can see four gain spectra. However, they coalesce into just two spectra with increasing values of the delay parameter.

It is also possible to observe up to five peaks for a given value of τ, which can correspond to multiple instability Raman bands. This is indeed the most relevant aspect of the noninstantaneous nonlinear parameter when both effects are taken into account, especially for the fast response regime (small τ). It is also possible to observe some sporadic peaks, breaking the smoothness of some spectra (Fig. 5).

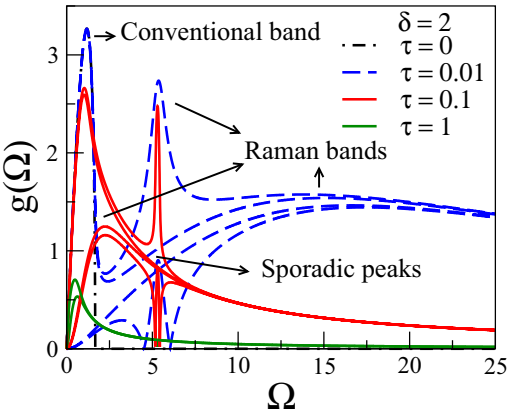

FIG. 5. MI gain spectra g (m^{-1}) as a function of the frequency Ω (THz) with the effect of noninstantaneous Kerr response for different values of τ (ps) for $\delta = 2\,ps\,m^{-1}$. The other parameters are the same as those used in previous figures.

However, for a better understanding of the phenomenological transition from fast to slow noninstantaneous response we have performed a more detailed study in Fig. 6, where it can be seen that the analysis is richer when both effects take place simultaneously.

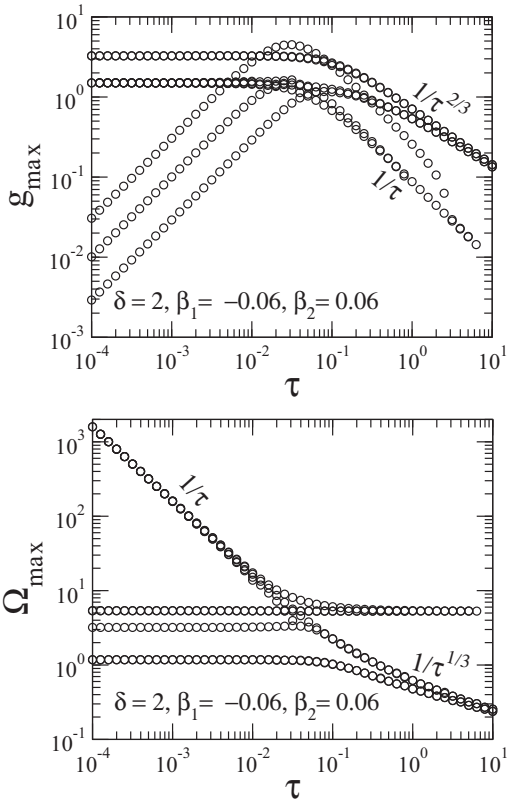

FIG. 6. Local maximum gain g_{max} (m^{-1}) and its corresponding frequency Ω_{max} (THz) for each instability branch as a function of the response time τ (ps) and null GVM ($\delta = 2\,ps\,m^{-1}$) for the case of mixed GVD regimes (circles). The other parameters are the same as those used in previous figures.

We plot [Fig. 6 (top)] the local maximum gain and its corresponding frequency for each instability branch as a function of the response time τ, for $\delta = 2$ ps m^{-1} as a prototype case. It is easy to identify a turnover point for $\tau^* \approx 0.005$ ps delimiting two well distinct trends. For $\tau < \tau^*$, $g_{\max}(\Omega) \sim \tau$, increasing linearly with τ. On the other hand, for $\tau > \tau^*$, $g_{\max}(\Omega)$ decreases with τ in two different forms: as $1/\tau$ for the smaller peaks and proportional to $1/\tau^{3/4}$ for the larger values of $g_{\max}(\Omega)$. The sporadic peaks decay in a fashion which is intermediate between these two tendencies, as illustrated in Fig. 6 (top) for $\tau > 0.05$. Another important feature is that the global maximum value of $g_{\max}(\Omega)$ as well as its second largest maximum remain unaltered in the regime of fast nonlinear response, decaying only when τ reaches the turnover point.

The corresponding frequencies in which the peaks take place are shown in Fig. 6 (bottom). One can verify that the greater the frequency, the faster it decreases with τ. Once again, the main role played in increasing the delayed response over the frequencies is to move them towards lower values until these Raman bands eventually fade out for sufficient large values of τ. We still identify the same threshold for $\tau = \tau^* \approx 0.05$, delimiting two different decaying slopes for $\Omega_{\max}$. For $\tau < \tau^*$, $\Omega_{\max}$ decays as $1/\tau$ for the frequencies related to the Raman bands (which occur for the higher frequencies).

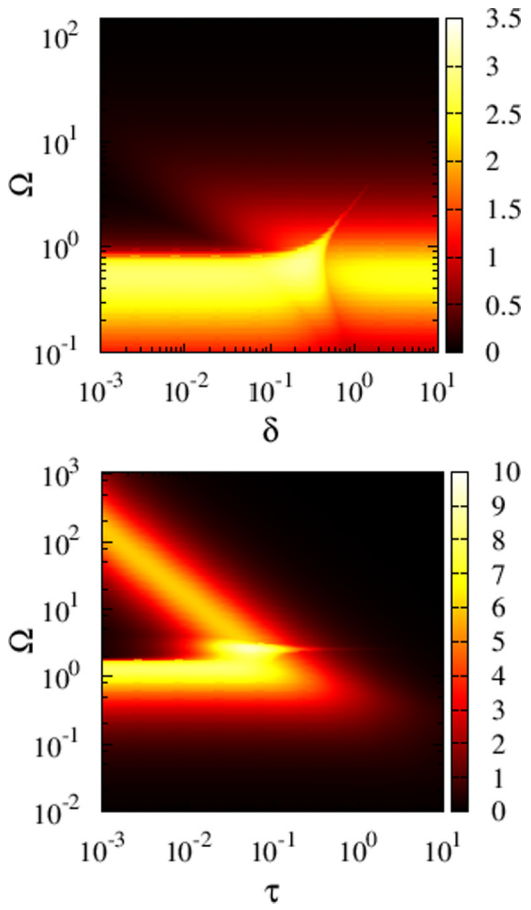

FIG. 7. Top: Total gain as a function of both the frequency Ω (THz) and the GVD δ (ps m)$^{-1}$ for $\tau = 1$ ps (top). Total gain as a function of nonlinear response time τ (ps) for the $\delta = 1$ ps m^{-1} (bottom).

Observe that, in this fast regime, the frequencies related to the conventional band, second largest and sporadic peaks remain independent of τ. On the other hand, for $\tau > \tau^*$, $\Omega_{\max}$ is merged in just two characteristic curves; one remains constant and the other decays as $1/\tau^{1/3}$.

In order to have an overview of the interplay between the XPM and the nonlinear response time on MI, we report in Fig. 7 a color plot of the total gain (the sum of all unstable modes) as a function of both frequency Ω and response time τ. Figure 7 (top) shows the overall effect of the GVM over the gain spectra. Its main effect is to reduce the width of the spectra as δ increases. Analyzing Fig. 7 (bottom), we can clearly see the two gain bands for fast responding media. The first band at low frequencies is due to the inherent instability of instantaneously responding media. The second one at larger frequencies is the Raman band. This plot shows clearly the shift of the Raman band as the response time increases up to the final coalescence of these instabilities in the slowing responding regime, after some turnover point. For τ sufficiently large, the modulation gain vanishes. In its central portion, it is possible to identify a minor distortion caused by the sporadic peaks.

IV. SUMMARY AND CONCLUSIONS

In summary, we have investigated the modulation instability in optical fibers with delayed Kerr nonlinearity and subjected to XPM in virtue of the coupling due to the intensity-dependent refractive index for two copropagating optical beams with the same polarization, but experiencing mixed GVD regimes. We modeled this system by incorporating time-dependent nonlinearities in the nonlinear Schrödinger equation governing the time evolution of the field envelopes. The dynamical equations for the nonlinear contributions were assumed to be relaxational. By considering small harmonic perturbations to the stationary solutions, we obtained the exact dispersion relation for the components of the perturbation fields that includes both the XPM and relaxation effects.

We unveiled that the case of fields copropagating in the mixed GVD regime presents quite new features associated with the MI gain spectrum as compared with the copropagation regime in with both fields experience normal GVD. We showed that, in the limit of an instantaneuous nonlinear response, the typical frequency with maximum gain converges to a finite value in the mixed GDV regime, while it continuously grows with the group-velocity mismatch in the normal GVD regime. As a result, the maximum gain typically decreases with the group-velocity mismatch in the mixed regime, contrasting with the opposite trend in the normal GVD regime.

The above features are directly related to the single- and double-band structures of the gain spectrum in the normal and mixed regimes, respectively. In the case of a noninstantaneous response, there are twice more harmonic modes exhibiting MI gain in the mixed than in the normal GVD copropagation regime. The MI gain spectrum displays four degenerated harmonic modes for fast nonlinear responses and two degenerated modes for the slow responding regime. Hence, it depicts distinct aspects in media with fast and slow delayed nonlinear responses. In media with fast nonlinear responses, there is a well-defined instantaneous gain band and multiple Raman bands associated with each degenerate unstable mode.

In slowly responding media, the Raman bands are shifted to lower frequencies and can suppress the instantaneous gain band.

The cases of small and large group-velocity mismatches also show distinct features, with the instantaneous gain band being displaced to lower frequencies as the group-velocity mismatch increases. The dependencies on the typical nonlinear response time τ and on the group-velocity mismatch δ of the main characteristics of the gain bands were also reported and showed distinct scaling behaviors in the small and large τ regimes. In particular, besides the mode having maximum gain at a frequency decaying with $1/\tau^{1/3}$, there is a second mode having maximum gain with a distinct scaling behavior $\Omega_{\max} \propto 1/\tau$ in the absence of group-velocity mismatch. The associated maximum gains scale, respectively, as $1/\tau^{2/3}$ and $1/\tau$, thus signaling the corresponding quadratic and linear dispersion relation of these modes in the low-frequency limit.

The present investigation sheds a new light on studies of ultrashort pulse propagation in nonlinear optical media with finite response times, as well as provides some motivation in manufacturing materials which account for the phenomenology exposed here. Along this direction, photonic crystal fibers filled with molecular liquids have been shown to exhibit a highly noninstantaneous response [63]. Wave propagation in such media depicts novel soliton solutions [49]. The interplay between the slow nonlinear response and balanced gain or loss contributions have been suggested as a possible mechanism to develop a passively mode-locked soliton laser [64]. The present results show that cross-phase modulation can strongly influence the modulational instability process in such slowly responding media. Considering that modulational instability is the underlying mechanism triggering soliton formation, further studies incorporating the joint effects of a delayed nonlinear response and gain or loss contributions would be in order to unveil their competing effects on the mechanism of soliton formation of copropagating beams in noninstantaneous nonlinear media.

ACKNOWLEDGMENTS

We are thankful for the partial financial support by CNPq, CAPES, UFAL, and the Alagoas State Research Agency FAPEAL through major projects (PPP-20110902-011-0025-0069 and 60030-733/2011). A.C. also acknowledges a PDE (CNPq) 207360/2014-6 and H. Eugene Stanley for the hospitality at the Center for Polymer Studies at Boston University where part of this work was done. B.L.B. acknowledges the hospitality of Eric J. Heller at Harvard University and financial support from CNPq, Grant No. 200540/2014-9.

[1] A. L. Moura, J. S. Aitchison, M. T. Araujo, and M. V. D. Vermelho, J. Appl. Phys. **100**, 033509 (2006).
[2] A. L. Moura, E. M. Nascimento, M. T. Araujo, M. V. D. Vermelho, and J. S. Aitchison, J. Appl. Phys. **105**, 036106 (2009).
[3] G. P. Agrawal, *Nonlinear Fiber Optics* (Academic, San Diego, 2007).
[4] V. E. Zakharov and L. A. Ostrovsky, Physica D **238**, 540 (2009).
[5] A. Hasegawa and F. Tappert, Appl. Phys. Lett. **23**, 142 (1973).
[6] A. Hasegawa and F. Tappert, Appl. Phys. Lett. **23**, 171 (1973).
[7] M. Wu and B. A. Kalinikos, Phys. Rev. Lett. **101**, 027206 (2008).
[8] M. Onorato, A. R. Osborne, and M. Serio, Phys. Rev. Lett. **96**, 014503 (2006).
[9] D. R. Solli, C. Ropers, P. Koonath, and B. Jalali, Nature (London) **450**, 1054 (2007).
[10] M. Stepić, A. Maluckov, M. Stojanović, F. Chen, and D. Kip, Phys. Rev. A **78**, 043819 (2008).
[11] N. Vishnu Priya and M. Senthilvelan, Wave Motion **54**, 125 (2015).
[12] V. V. Konotop and M. Salerno, Phys. Rev. A **65**, 021602 (2002).
[13] L. D. Carr and J. Brand, Phys. Rev. Lett. **92**, 040401 (2004).
[14] K. L. Henderson, K. L. Peregrine, and J. W. Dold, Wave Motion **29**, 341 (1999).
[15] M. Onorato, A. R. Osborne, M. Serio, and S. Bertone, Phys. Rev. Lett. **86**, 5831 (2001).
[16] A. Picozzi, S. Pitois, and G. Millot, Phys. Rev. Lett. **101**, 093901 (2008).
[17] B. Kibler, C. Michel, A. Kudlinski, B. Barviau, G. Millot, and A. Picozzi, Phys. Rev. E **84**, 066605 (2011).
[18] J. Fatome, S. Pitois, and G. Millot, Opt. Fiber Technol. **12**, 243 (2006).
[19] N. Da Dalt, C. De Angelis, G. F. Nalesso, and M. Santagiustina, Opt. Commun. **121**, 69 (1995).
[20] Y. D. Gong, P. Shum, D. Tang, C. Lu, and X. Guo, Opt. Express **11**, 2480 (2003).
[21] A. M. Rubenchik, S. K. Turitsyn, and M. P. Fedoruk, Opt. Express **18**, 1380 (2010).
[22] M. Centurion, M. A. Porter, Y. Pu, P. G. Kevrekidis, D. J. Frantzeskakis, and D. Psaltis, Phys. Rev. A **75**, 063804 (2007).
[23] F. Amrani, B. Kibler, P. Grelu, S. Wabnitz, S. Trillo, and G. Millot, Opt. Lett. **38**, 5327 (2013).
[24] G. Genty, M. Lehtonen, and H. Ludvigsen, Opt. Express **12**, 4614 (2004).
[25] I. Velchev, R. Pattnaik, and J. Toulouse, Phys. Rev. Lett. **91**, 093905 (2003).
[26] S. Abdoulkary, A. D. Aboubakar, M. Aboubakar, A. Mohamadou, and L. Kavitha, Commun. Nonlinear Sci. Numer. Simul. **22**, 1288 (2015).
[27] P. Tchofo Dinda and K. Porsezian, J. Opt. Soc. Am. B **27**, 1143 (2010).
[28] K. Nithyanandan, R. V. Raja, K. Porsezian, and B. Kalithasan, Phys. Rev. A **86**, 023827 (2012).
[29] K. W. Chow, K. K. Y. Wong, and K. Lam, Phys. Lett. A **372**, 4596 (2008).
[30] L. Zhang, Y. Xiang, X. Dai, and S. Wen, J. Opt. Soc. Am. B **31**, 3029 (2014).
[31] A. K. Shafeeque Ali, K. Nithyanandan, and K. Porsezian, Phys. Lett. A **379**, 223 (2015).

[32] A. Biswas, K. R. Khan, M. F. Mahmood, and M. Belic, Optik **125**, 3299 (2014).
[33] Y. Xianq, X. Dai, S. Wen, and D. Fan, J. Opt. Soc. Am. B **28**, 908 (2011).
[34] W. Zhou, W. Su, X. Cheng, Y. Xiang, X. Dai, and S. Wen, Opt. Commun. **282**, 1440 (2009).
[35] X. Zhong, K. Cheng, and S. Chiang, J. Opt. Soc. Am. B **31**, 1484 (2014).
[36] M. L. Lyra and A. S. Gouveia Neto, Opt. Commun. **108**, 117 (1994).
[37] X. Zhong and A. Xiang, Opt. Fiber Technol. **13**, 271 (2007).
[38] G. L. da Silva, I. Gleria, M. L. Lyra, and A. S. B. Sombra, J. Opt. Soc. Am. B **26**, 183 (2009).
[39] G. L. da Silva, A. A. Canabarro, and B. de Lima Bernardo, Ann. Phys. (NY) **363**, 476 (2015).
[40] A. A. Canabarro, B. Santos, I. Gleria, M. L. Lyra, and A. S. B. Sombra, J. Opt. Soc. Am. B **27**, 1878 (2010).
[41] G. L. da Silva, T. P. Lobo, and A. A. Canabarro, J. Opt. Soc. Am. B **31**, 2012 (2014).
[42] C. Cambournac, H. Maillotte, E. Lantz, J. M. Dudley, and M. Chauvet, J. Opt. Soc. Am. B **19**, 574 (2002).
[43] M. J. Potasek, Opt. Lett. **12**, 921 (1987).
[44] X. Liu, J. W. Haus, and S. M. Shahriar, Opt. Commun. **281**, 2907 (2008).
[45] K. Nithyanandan and K. Porsezian, Opt. Commun. **303**, 46 (2013).
[46] S. Trillo, S. Wabnitz, G. I. Stegeman, and E. M. Wright, J. Opt. Soc. Am. B **6**, 889 (1989)
[47] G. Carbou and B. Hanouzet, Commun. Math. Sci. **4**, 331 2006.
[48] C.-S. Chou and M.-F. Shih, J. Opt. A, Pure Appl. Opt. **11**, 105204 (2009).
[49] C. Conti, M. A. Schmidt, P. St. J. Russell, and F. Biancalana, Phys. Rev. Lett. **105**, 263902 (2010).
[50] I. Fushman and J. Vuckovic, Opt. Express **15**, 5559 (2007).
[51] S. R. Friberg, S. Machida, and Y. Yamamoto, Phys. Rev. Lett. **69**, 3165 (1992).
[52] S. L. Braunstein and P. V. Loock, Rev. Mod. Phys. **77**, 513 (2005).
[53] P. Grangier, J. A. Levenson, and J.-P. Poizat, Nature (London) **396**, 537 (1998).
[54] P. D. Drummond, R. M. Shelby, S. R. Friberg, and Y. Yamamoto, Nature (London) **365**, 307 (1993).
[55] G. P. Agrawal, Phys. Rev. Lett. **59**, 880 (1987).
[56] G. P. Agrawal, P. L. Baldeck, and R. R. Alfano, Phys. Rev. A **39**, 3406 (1989).
[57] M. Yu, C. J. McKinstrie, and G. P. Agrawal, Phys. Rev. E **48**, 2178 (1993).
[58] T. Tanemura and K. Kikuchi, J. Opt. Soc. Am. B **20**, 2502 (2003).
[59] A. S. Gouveia-Neto, M. E. Faldon, A. S. B. Sombra, P. G. J. Wigley, and J. R. Taylor, Opt. Lett. **13**, 901 (1988).
[60] D. Schadt and B. Jaskorzynska, Electron. Lett. **23**, 1090 (1987).
[61] E. Kengne, S. T. Chui, and W. M. Liu, Phys. Rev. E **74**, 036614 (2006).
[62] A. Armaroli and S. Trillo, J. Opt. Soc. Am. B **31**, 551 (2014).
[63] R. V. J. Raja, A. Husakou, J. Hermann, and K. Porsezian, J. Opt. Soc. Am. B **27**, 1763 (2010).
[64] N. N. Akhmediev, M. J. Lederer, and B. Luther-Davies, Phys. Rev. E **57**, 3664 (1998).